1

General introduction

Abstract.
The aim of this thesis is to characterize a well verifiable metal-halide (MH) lamp and obtain a set of reliable measurement data. The experimentally obtained data is used to validate existing numerical models of the MH lamp, which gain a better understanding of the plasma properties and transport phenomena in the MH lamp. In this thesis we study the additive distribution and the resulting light output of the lamp. Axial segregation of the additive, which is caused by the combination of the convective and diffusive phenomena in the lamp, is investigated. Convection is induced by gravity and therefore the lamp was measured under varying gravity conditions. In this thesis measurements during parabolic flights and in a centrifuge are presented. The diagnostics to investigate the lamp are laser absorption spectroscopy, the newly developed Imaging Laser Absorption Spectroscopy, and emission spectroscopy. The results are used as input for a numerical model of the same lamp.

Parts of this chapter have been submitted, in altered form, as [A.J. Flikweert, T. Nimalasuriya, G.M.W. Kroesen, M. Haverlag and W.W. Stoffels, *The metal-halide lamp under varying gravity conditions measured by emission and laser absorption spectroscopy*, Microgravity Science and Technology (2008)].

Worldwide, 20% of all electricity is used for lighting [1–3]. For this reason, efficient lamps are economically and ecologically important.

1.1 Incandescent lamps

The first practical lamp, based on a carbon filament, was made by Edison in 1876. The filament acts as a resistor, heats up and radiates light. Later on, it turned out that tungsten is the best material for the filament. Due to the good colour rendering of the incandescent lamp and the simple design, they are still widely used in domestic applications.

The efficiency and the life time were increased by the introduction of the halogen lamp. Halogen lamps are also still widely used, for instance in car headlamps and shop lighting.

The physical process behind the generation of light by incandescent lamps is black body radiation. Ideally, the power loss is dominated by this black body radiation [4], but conduction can also be important. A large part of the radiation is in the infrared and not in the visible. This results in efficiencies of about 4% for incandescent lamps, which is one of the worst of all lamps. A more efficient way to generate light is by using a plasma.

1.2 Gas discharges

In gas discharge lamps, plasma is created by the electrical current flowing through the gas. Plasma can be seen as the fourth state of matter, besides solid, liquid and gas. In the universe, about 99% of the visible material is plasma.

A plasma is an ionized gas. It contains free electrons, ions and sometimes charged clusters or dust particles. Because of the charged particles, a plasma conducts electricity and particles can be excited and radiate light. A plasma usually has a temperature of several thousands or ten thousands of degrees. Therefore, plasma is not abundant on earth. In the universe, plasma is abundant in the form of stars and interstellar nebulae. On earth, examples of plasmas are (ball) lightning, the aurora and a candle flame.

Plasmas are created by men for several purposes. In this section, some applications of low- and high-pressure discharges are given.

1.2.1 Low-pressure discharges

In low-pressure discharges (pressure below 1 bar), the collision frequency between electrons and heavy particles is low, so electrons can remain at a high temperature, whereas the heavy particles remain relatively cool due to contact with the wall. This means that the plasma is not in local thermodynamical equilibrium (LTE). Due to the high

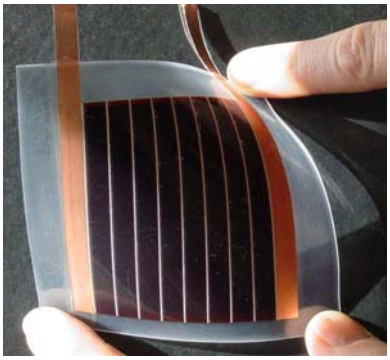

Figure 1.1: Example of a plasma produced flexible solar cell, made by Akzo Nobel [6].

electron temperature, the plasma is chemically active. Many applications are based on the reactive plasmas, like plasma deposition, etching and surface modification.

An example of plasma deposition is the production of thin-film solar cells within the Helianthos project [5, 6]. For the production of flexible, thin-film solar cells, a roll-to-roll machine is used. The technique for deposition of the various layers on the film is plasma-enhanced chemical vapour deposition. The plasma is a silane (SiH_4) plasma; dopants are added to obtain the various active layers of the solar cell. Figure 1.1 shows a picture of a plasma produced flexible solar cell.

Another application of a low-pressure discharge is a thruster based on plasma. A thruster is used as engine in space, for instance for interplanetary travel and altitude control of satellites. The requirements for a thruster are a low propellant consumption and a high energy efficiency. The Helicon Double Layer Thruster is developed at the Australian National University (ANU) [7–15] and meets these requirements. The thruster accelerates the propellant to about 15 km s^{-1}, gaining momentum in the mN range. The propellant in this thruster is argon. The argon plasma is created using a helicon system. A current-free double layer is created; the potential drop in this layer accelerates the argon ions. A schematic drawing of Chi Kung, a horizontal helicon system, is shown in figure 1.2.

Regarding lighting, examples of low-pressure discharge lamps are compact fluorescent lamps (also known as energy-saving lamps) and fluorescent tubes. They have better efficiencies (20%–30%) then incandescent lamps and longer lifetimes. These lamps contain mercury. Mercury is an efficient radiator, but radiates in the UV. The phosphor coating in the fluorescent tubes converts the UV to the visible, but about half of the photon energy is lost in this conversion (the so-called Stokes losses). Another example is the well-known low-pressure sodium lamp (deep orange street lighting), which has a slightly lower discharge conversion efficiency, but the 589 nm line is around the

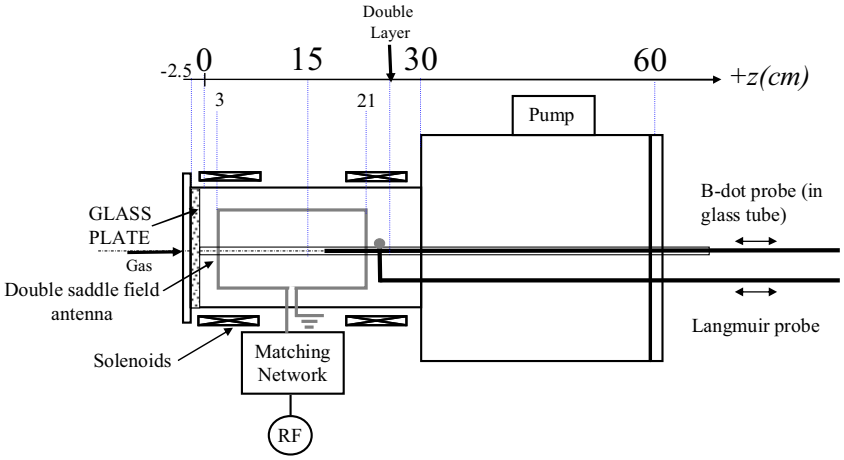

Figure 1.2: Schematic overview of Chi Kung, a horizontal helicon system at the ANU [8]. The power is inductively coupled by a double saddle antenna. The gas inlet is at the left, whereas the pump is at the right vessel. At the position of the expansion of the plasma (between the narrower launch vessel and the wider expansion vessel) a double layer is formed, where the Ar ions are accelerated. The measurement techniques to investigate the plasma are a $\dot{B}$ probe [16] and a Langmuir probe.

maximum of the human eye's sensitivity. Therefore, no phosphor is needed, resulting in a higher efficiency. The monochromatic light limits the application of the low-pressure sodium lamp.

1.2.2 High-pressure discharges

In high-pressure discharges (atmospheric pressure, or above 1 bar), the collision frequency between electrons and heavy particles is high.

Examples of atmospheric-pressure discharges are corona discharges [17] and the plasma needle with biomedical applications [18, 19]. The plasma needle is applied directly on organic materials and living tissues [20]. Possible applications are high-precision removal of unwanted cells and use in dentistry to clean dental cavities, prior to filling. The plasma is small enough (∼1 mm) for local surface treatment.

In lighting, High Intensity Discharge (HID) lamps are high-pressure discharges based on arc emission [3, 21–26]. HID lamps are efficient lamps with often a good colour rendering index. The first HID lamps were mercury lamps at atmospheric pressure. They also emit UV which is converted by a phosphor into visible light, but the ratio of visible to UV is greater than for the fluorescent tubes. A better white lamp is obtained when salt additives (metal halides) are added to the mercury lamp. These

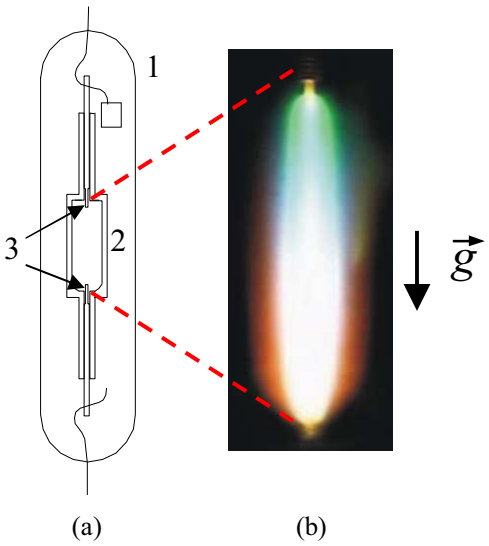

Figure 1.3: (a) Schematic picture of the COST reference lamp [27], (1) outer bulb; (2) burner (size 8 mm x 20 mm); (3) electrodes, distance between both electrodes ∼16 mm. (b) The burner of a MH lamp (contains 10 mg Hg and 4 mg DyI_3), colour segregation is clearly visible.

lamps are known as metal-halide (MH) lamps. MH lamps have a high efficiency (up to 40%) [3] and emit white light. They are mainly used for applications where a high light output is desired; examples are shop lighting, street lighting, flood lighting of sport stadiums and city beautification.

1.3 Metal-halide lamp

1.3.1 The COST reference lamp

The MH lamps we use are MH reference lamps developed within the European COST action program 529 [27]. The definition of a standard laboratory MH lamp allows us to get comparable results from the worldwide available diagnostic and modelling techniques for MH lamps. A schematic drawing of the lamp is given in figure 1.3(a). The diameter of the lamp burner is 8 mm and the burner height is 14 to 20 mm. The electrode distance is 8 or 16 mm. The lamp contains Ar/Kr^{85} as starting gas, Hg as buffer gas and a salt additive (we mainly use DyI_3). When the lamp is ignited, the Hg evaporates and a mercury discharge is created. The lamp heats up and the salt additive enters the arc discharge.

1.3.2 Axial segregation

When the lamp is burning vertically, segregation of the additives occurs [27, 28] and colour segregation appears. This limits the lamp design for application in, for example, shop lighting; these lamps are oriented in various direction. Figure 1.3(b) shows an image of the plasma when the lamp is burning. The bluish-white light at the bottom is caused by Dy atoms, whereas the bluish colour at the top is caused by Hg atoms. This non-uniform light output has a bad influence on the efficiency and the colour rendering of the lamp.

For the case of DyI_3 as salt additive the situation is as follows. The centre of the arc is much hotter (∼5500 K) than the wall (∼1200 K) [29]. First we have convection because of this large gradient. Convection is induced by gravity. The hot gas in the centre moves upward, whereas the colder gas near the wall moves downward.

Because of the large temperature gradient a multi-step process of dissociation of DyI_3 molecules near the centre and association of atoms at the wall takes place [30]:

$$\mathrm{DyI_3} \rightleftarrows \mathrm{DyI_2} + \mathrm{I} \rightleftarrows \mathrm{DyI} + 2\mathrm{I} \rightleftarrows \mathrm{Dy} + 3\mathrm{I}. \tag{1.1}$$

With increasing temperature the equilibrium moves to the right-hand side. Furthermore in the centre of the burner, ionization of Dy atoms takes place because of the high temperature [31]:

$$\mathrm{Dy} + e \rightleftarrows \mathrm{Dy}^+ + e + e. \tag{1.2}$$

Due to the different diffusion velocities of the heavier molecules and the lighter atoms and ions, the molecules move slower inward than the atoms and ions move outward. This causes a hollow radial pressure profile of atoms: radial segregation. Note that this is in addition to the ideal gas law $p = nkT$; a higher temperature gives a lower density.

While the Dy atoms are moving outward and get closer to the wall, they are dragged downward by the convection. In this way the Dy atoms stay mainly at the bottom of the lamp. The combination of convection and radial segregation thus causes axial segregation in the lamp as seen in figure 1.3(b). The representative flow lines of the atomic dysprosium are drawn in figure 1.4.

Axial segregation of Dy is thus caused by the combination of convection and diffusion. When the time scales of these effects are in the same order of magnitude, maximal axial segregation occurs. In the limiting cases, when the convection is absent or when the convection is much stronger than diffusion, good mixing is observed: no axial colour segregation is observed in the lamp. E. Fischer [28] developed a theory for an infinitely long lamp which gives the amount of segregation as a function of the amount of convection, which is depicted in figure 1.5. Because the convection is induced by gravity, measuring under different gravity conditions aids the understanding of the diffusive and convective processes.

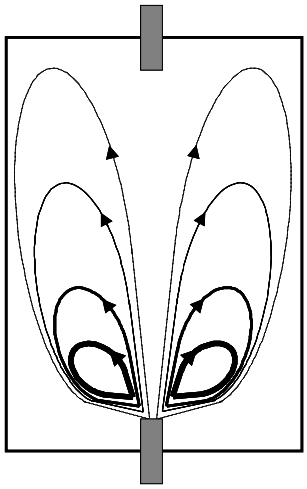

Figure 1.4: Schematic of the flow lines of atomic dysprosium in the burner. Thick lines represent a high dysprosium density whereas thin lines represent a low density [32].

1.4 Varying gravity conditions

Convection in the MH lamp is caused by gravity and to gain more insight in the flow phenomena, the lamp is investigated under varying gravity conditions. Besides laboratory experiments ($1g$, where g is the gravity at earth: 9.81 m s^{-2}) [32, 34–36], the lamp is investigated during parabolic flights. Here the lamp is measured during periods of about 20 s of micro-gravity ($0g$) and hyper-gravity ($\sim 1.8g$) [33]. Finally the lamp is placed in a centrifuge (1–$10g$) [35, 37–39]. This centrifuge is used as a tool to vary the (artificial) gravity and thus the amount of convection for a longer time than at the parabolic flights to assure stable arc conditions.

1.4.1 Parabolic flights

During the parabolic flights, the dynamic lamp behaviour is investigated to obtain a relationship between the gravity and atomic Dy density in the lamp. The lamp has been measured during the parabolic-flight campaign of the European Space Agency (ESA) in June 2004 [40]. During each flight, 31 parabolas with micro-gravity and hyper-gravity were performed. Figure 1.6 shows one parabola schematically.

For a thorough investigation of the lamp the periods are also too short. Therefore a centrifuge was built, where hyper-gravity can be prolonged.

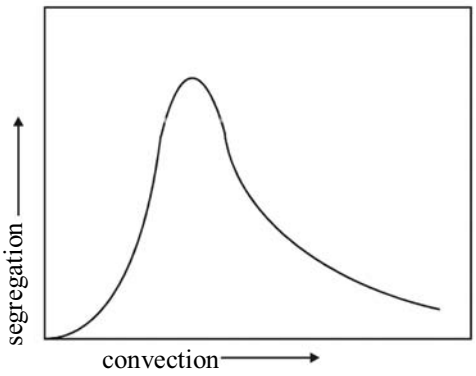

Figure 1.5: The Fischer curve [28, 33] which gives the amount of axial segregation as a function of the amount of convection. Convection is induced by gravity. At $1g$, where g is the gravity at earth (9.81 m s^{-2}), our lamps are around the maximum of the curve.

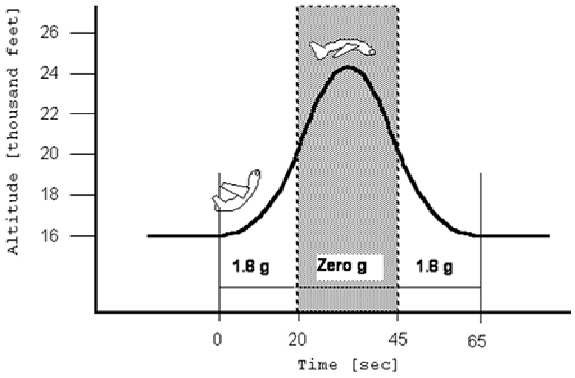

Figure 1.6: Sequence of a parabola: first hyper-gravity ($\sim$ 20 s), next micro-gravity ($\sim$ 25 s) and finally again hyper-gravity [33, 40].

1.4.2 The centrifuge

A centrifuge was built to investigate the lamp under hyper-gravity conditions [37]. The gravity that is achieved by the centrifuge ranges from 1–10g.

A schematic representation of the centrifuge is given in figure 1.7. The centrifuge consists of a pivot, an arm and a gondola attached to the arm. The gondola contains all electrical equipment and the measurement setup (including lamp) itself. The total diameter at maximum swing-out of the gondola is about 3 m. The maximum rotation

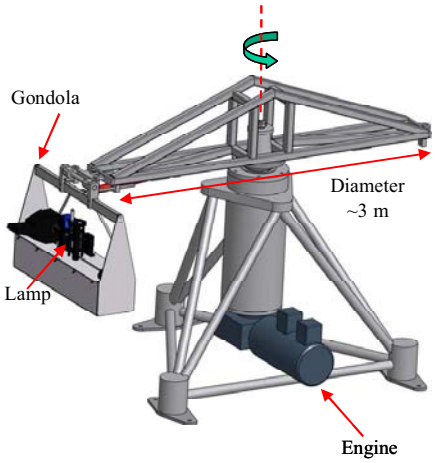

Figure 1.7: Schematic representation of the centrifuge. It consists of a pivot, an arm and the gondola that contains the lamp and diagnostics [37].

frequency is $\sim$ 1.5 Hz which corresponds to a velocity of 50 km h^{-1}. The gondola swings out around its hinge point when spinning the centrifuge, so the artificial gravity vector is always parallel to the lamp axis.

The measurement system in the centrifuge is shown in figure 1.8. We use a control PC outside the centrifuge laboratory. This PC drives the frequency controller of the centrifuge engine. The gondola contains another (mini-) computer on which the experimental software is running. The experimental software is written in National Instruments LabWindows/CVI. In addition to this computer, the gondola contains all the equipment: the lamp power supply, a CCD camera, an ordinary webcam, the laser controller and a data acquisition system. The lamp and diagnostics are on the rail on top of the gondola. The computer inside the gondola is connected to the control PC by the wireless network. The only fixed connection (slip ring) to the outer world is the 230 V power wire. We use Windows Remote Desktop to operate the gondola PC. During the measurements, the gondola PC collects the data on its flash disks. After the measurements are finished, the data is transferred to the control PC and the data is processed off-line.

The lamp is monitored on-line by a simple webcam. From the webcam images, colour segregation can be observed clearly. Figure 1.10 shows various webcam images of a lamp with 10 mg Hg and 4 mg of DyI_3 [39]. The input power is 150 W. A picture taken at $0g$ is displayed for comparison. This picture was taken during experiments in the International Space Station (ISS) [41]. The other images are taken at the centrifuge setup. At $0g$ no axial segregation is present; we are at the origin of the Fischer curve

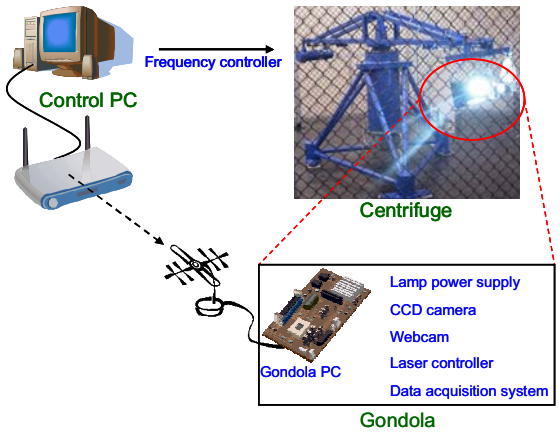

Figure 1.8: The measurement system in the centrifuge. The equipment in the centrifuge gondola is controlled by a mini-computer, which is connected via wireless network to the control PC.

(figure 1.5). At $1g$ we are in the area of the maximum of the curve. Increasing the gravity means increasing the convection and thus moving to the right on the Fischer curve. This is observed in the pictures: when gravity is increased, better mixing occurs and axial segregation is diminished.

1.5 Diagnostics

In this section the diagnostics are discussed. Laser absorption spectroscopy has been used in laboratory experiments and during parabolic flights. The Imaging Laser Absorption Spectroscopy (ILAS) technique is an extension of the laser absorption technique. The ILAS technique is used in the experiments under hyper-gravity in the centrifuge. Finally emission spectroscopy is discussed.

1.5.1 Laser absorption spectroscopy (1D)

In the measurements in the laboratory and during the parabolic flights, we use laser absorption spectroscopy. The beam of a diode laser is expanded to a sheet. When it illuminates the lamp, part of the light is absorbed by the dysprosium atoms. After the lamp and optics the laser light hits a diode array, which measures the remaining intensity of the laser light. In this way, a line-of-sight density profile of atomic ground state dysprosium is obtained at one axial position of the lamp (one-dimensional, 1D), which gives a measure for the amount of axial segregation. In the laboratory experiments,

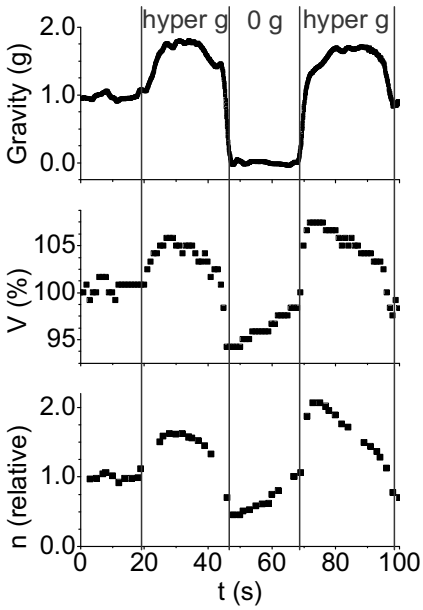

Figure 1.9: Gravity, lamp voltage and radially averaged ground state atomic Dy density for a lamp with 10 mg Hg and 4 mg DyI_3 during one parabola, as functions of time [33].

the lamp is measured at several axial positions; a 2D density profile is constructed from these 1D measurements.

During the parabolic flights, the Dy density in the lamp and the voltage over the lamp (which is proportional to the total amount of Dy in the arc) are measured during a parabola. Figure 1.9 shows an example of the density and voltage of the lamp with 4 mg DyI_3 and 10 mg Hg, at 150 W input power. The values given in this graph are relative values; the atomic ground state Dy density is in the order of 10^{21} m^{-3} and the voltage is $\sim$80 V. The increase in Dy density at the first hyper-gravity phase is explained by a better mixing and thus less axial segregation above $1g$. This is because we are at the right-hand side of the Fischer curve (figure 1.5) [32, 33, 41]. However, it is seen that at the end of the micro-gravity phase, the Dy density is still not constant. This is because the diffusion time constant is larger than the 25 s of micro-gravity. This problem does not occur in the ISS, where we have micro-gravity for a period much longer than during the parabolic flights.

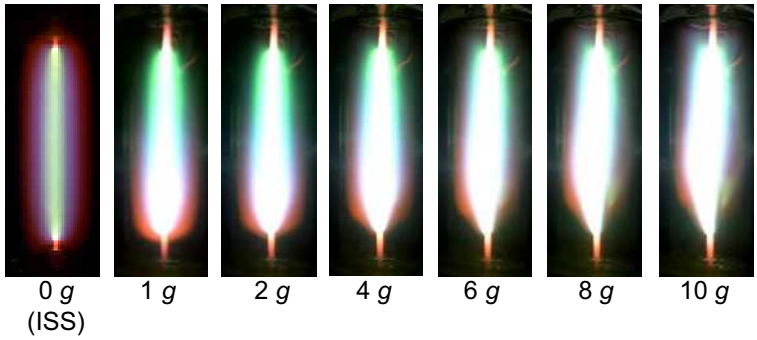

Figure 1.10: Pictures of the lamp at 0–10g. The first image is taken in the ISS [41], the others are taken in the centrifuge setup [37, 39]. Note that the exposure time of the ISS picture is different from those at the centrifuge.

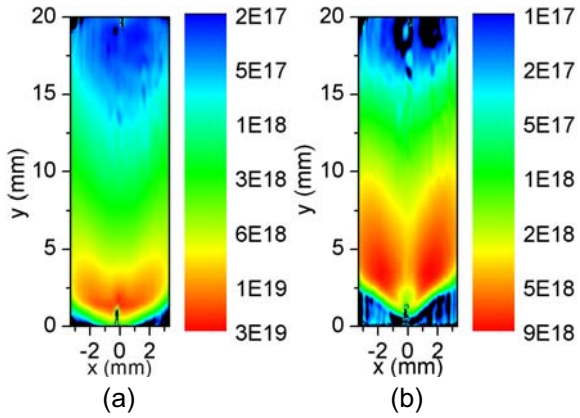

Figure 1.11: Atomic ground state Dy density measured by ILAS [37], $P = 150$ W, 5 mg Hg and 4 mg DyI_3, (a) 1g; (b) 10g. Note that the flame-like pattern at the top of the lamp is an artefact caused by the data analysis.

1.5.2 Imaging Laser Absorption Spectroscopy (2D)

The Imaging Laser Absorption Spectroscopy (ILAS) technique [37] is an extension of the laser absorption technique. In contrast to the 1D laser absorption spectroscopy, ILAS yields the 2D density distribution of ground state atomic Dy. We use a diode laser and scan around an absorption line of atomic Dy (642.19 nm). The laser beam is expanded so it illuminates the whole lamp burner. While passing the lamp, the Dy atoms in the lamp absorb part of the beam. After the lamp and optics, the laser light is imaged

on a CCD camera. In this way, for each position in the lamp an absorption profile is constructed. From these profiles the atomic ground state Dy density is calculated so a 2D density plot is obtained.

The 2D density of ground state atomic Dy is shown for $1g$ and $10g$ in figure 1.11. The lamp filling is 5 mg Hg and 4 mg DyI_3; the input power is 150 W. These density profiles show that a better mixing occurs at $10g$: the amount of Dy at the top of the lamp is increased. This is consistent with the webcam images in figure 1.10, which show also a better mixing and thus less colour segregation at higher gravity.

1.5.3 Emission spectroscopy

The lamp is investigated by means of emission spectroscopy, which gives the line intensities of the different particles in the lamp. A 0.25 m spectrometer is placed in the gondola in the centrifuge. The lamp is focused on the entrance slit of the spectrometer. The entrance slit is in vertical direction; in this way an axial profile of the lamp is imaged on the spectrometer slit. After the spectrometer, the dispersed light hits a CCD camera. The image contains the wavelength in horizontal direction and the axial position in the lamp in vertical direction. In this way, we obtain axial intensity profiles of different species. These axial intensity profiles can be analyzed; in this way a measure for the axial segregation can be found.

T. Nimalasuriya *et al* [35, 41] built a more complex emission spectroscopy setup. The spectrometer used for the optical emission measurements is originally designed for the ISS: it has to be compact and lightweight. These requirements are met using a Echelle spectrometer. In this setup, the slit is in horizontal direction, yielding lateral emission profiles. By using this setup, the temperature profile of the lamp is obtained from a calibrated Hg line. After combining these temperature profiles with the calibrated Dy lines, absolute Dy densities are obtained.

The axial segregation that is observed by the webcam (figure 1.10) is also observed by emission spectroscopy. In figure 1.12 the intensity profiles of a Dy line are shown as a function of the lateral position in the lamp. These profiles are obtained at 3 axial positions in the lamp (10 mg Hg, 4 mg DyI_3, $P = 150$ W), for both normal gravity ($1g$) and $10g$. Note that the intensity profiles and webcam images were taken from different angles (90° with respect to each other) [37]. From the profiles at the bottom, we see that the amount of Dy decreases from $1g$ to $10g$. At the top we see an increase of the amount of Dy when increasing g; Dy is mixed better over the lamp (less axial segregation).

1.6 Thesis outline

This thesis deals with various diagnostic techniques to investigate the MH lamp. Together with the thesis of T. Nimalasuriya [35], which deals with a poly-diagnostic (ex-

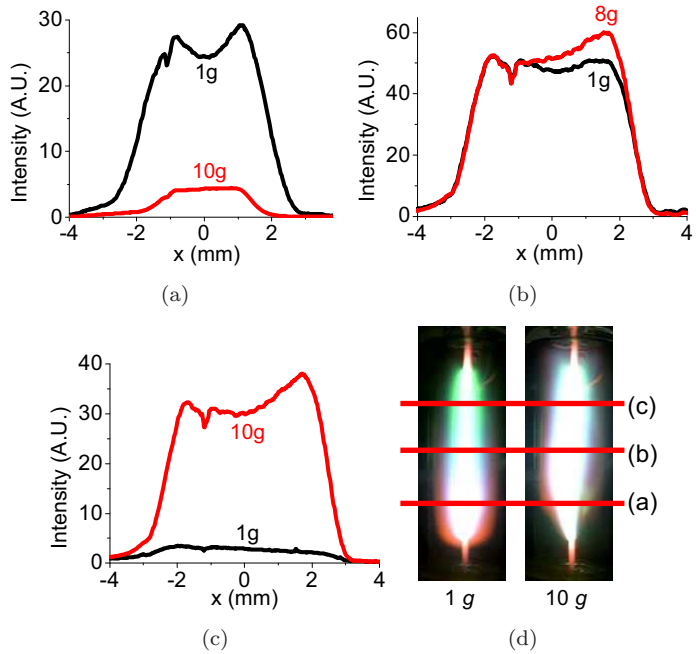

Figure 1.12: Atomic Dy line (642.19 nm) intensities at different axial positions in the lamp measured by emission spectroscopy, for normal and hyper-gravity [38]: (a) bottom; (b) centre; (c) top. In (d) the webcam images are given for comparison; the positions where the profiles were taken are indicated (printed in colour in figure 1.10).

perimental) study of the MH lamp and the thesis of M.L. Beks [42], which is about the modelling of the MH lamp, it presents a complete overview of the dominant processes which govern the segregation phenomena in MH lamps.

Chapter 2 presents laser absorption measurements on the MH lamp with DyI_3 at $1g$. The 1D laser absorption spectroscopy is discussed and some results of a MH lamp with 10 mg Hg and 4 mg DyI_3 are shown.

In chapter 3 the lamp is investigated during parabolic flights (0–$2g$). The diagnostics are 1D laser absorption spectroscopy, lamp voltage measurements, and integrated light output measurements. Three lamps with different amounts of Hg are compared.

Chapter 4 presents the centrifuge, which yields an acceleration between 1–$10g$. This chapter also describes the newly developed (2D) Imaging Laser Absorption Spectroscopy setup. This setup is developed from the knowledge of the 1D setup that is presented in chapters 2 and 3.

In the first ILAS measurements, a deviation from the Fischer model is observed. This

model assumes an infinitely long lamp with a constant axis temperature. In chapter 5, the axial segregation model by Fischer is extended for our lamps; real lamps have finite length and have an axial temperature gradient. This chapter also introduces some new parameters to characterize the lamp.

Chapter 6 presents ILAS measurements on the lamps and a thorough analysis of the obtained results. The measurements are under 1–10g. The centrifuge and the ILAS technique used to investigate the lamp have been introduced in chapter 4.

In addition to the ILAS measurements, emission spectroscopy measurements under 1–10g have been carried out on the same lamps in chapter 7. After validation of the measurement technique by comparing the results with those obtained in chapter 6, also commercially available lamps are investigated.

The results obtained by ILAS are compared to results obtained by numerical modelling. This is done in chapter 8. First the model is presented and some experimental results are compared with the results obtained by modelling. The last part of the chapter presents and compares two-dimensional images obtained by experiment and model.

Finally in chapter 9 we combine the conclusions of the different chapters, draw general conclusions, give an overview of the various introduced axial segregation parameters and give an outlook for future work.